

A Fluorescent Orthotopic Bone Metastasis Model of Human Prostate Cancer¹

Meng Yang, Ping Jiang, Fang-Xian Sun, Satoshi Hasegawa, Eugene Baranov, Takashi Chishima, Hiroshi Shimada, A. R. Moossa, and Robert M. Hoffman²

AntiCancer, Inc., San Diego, California 92111 [M. Y., P. J., F-X. S., S. H., E. B., R. M. H.]; Department of Surgery, University of California, San Diego, California 92103-8220 [M. Y., S. H., A. R. M., R. M. H.]; and Department of Surgery, Yokohama City University School of Medicine, Yokohama, Japan [M. Y., S. H., T. C., H. S.]

Abstract

Here, we report a fluorescent spontaneous bone metastatic model of human prostate cancer developed by surgical orthotopic implantation of green fluorescent protein (GFP)-expressing prostate cancer tissue. Human prostate cancer PC-3 cells were transduced with the pLEIN expression retroviral vector containing the enhanced GFP and neomycin resistance genes. Stable GFP high-expression PC-3 clones were selected *in vitro* with G418, which were then combined and injected s.c. in nude mice. For metastasis studies, fragments of a single highly fluorescent s.c. growing tumor were implanted by surgical orthotopic implantation in the prostate of a series of nude mice. Subsequent micrometastases and metastases were visualized by GFP fluorescence throughout the skeleton, including the skull, rib, pelvis, femur, and tibia. The central nervous system, including the brain and spinal cord, was also involved with tumor, as visualized by GFP fluorescence. Systemic organs, including the lung, plural membrane, liver, kidney, and adrenal gland, also had fluorescent metastases. The metastasis pattern in this model reflects the bone and other metastatic sites of human prostate cancer. Thus, this model should be very useful for the study and development of treatment for metastatic androgen-independent prostate cancer.

Introduction

Prostate cancer has become the most prevalent cancer diagnosed and the second leading cause of cancer death for North American men (1). Despite improvement in early detection, more refined diagnostic modalities, and a better understanding of the natural history of the disease, metastatic prostate cancer remains largely untreatable (2). Therefore, to gain further insight into and develop new therapeutics for human prostate cancer progression and bone metastasis in particular, an accurate *in vivo* model is essential.

Early experimental models involving implanting human prostate cancer cells s.c. in athymic nude mouse failed to yield metastatic disease (3). With the androgen-independent PC-3 human prostate cancer cell line as a model, which originated from a bone metastasis (4), osseous metastasis could be induced in nude mice by injecting tumor cells i.v. with concomitant occlusion of the inferior cava or by intracardiac implantation (5–7).

In orthotopic transplant models of human prostate cancer, Stephenson *et al.* (8), Fu *et al.* (9), Pettaway *et al.* (6), Saito *et al.* (10), Rembrink *et al.* (11), and An *et al.* (12) have observed prostate cancer metastasis but only in the lymph nodes and the lung. Thalmann *et al.* (13) reported a spontaneous bone metastasis model of androgen-independent human prostate cancer LNCaP-derived sublines. The animals developed bone metastasis in 10 and 21.5% of intact and castrated hosts, respectively, after orthotopic injection of cell suspen-

sions (13). These results provided some useful information to recognize the biological behavior of prostate cancer.

The early stages of tumor progression and micrometastasis formation have been difficult to visualize in current models due to the inability to identify small number of tumor cells against a background of many host tissues. We have developed new models of human and animal cancer by transfer of the *Aequorea victoria* jellyfish GFP³ gene to tumor cells, which enables visualization of fluorescent tumors and metastases at the microscopic level in fresh viable tissue after transplantation (14–19).

Here, high expression of GFP in the tumor cells in the surgical orthotopic implantation (SOI) model of androgen-independent PC-3 human prostate cancer has revealed the very extensive and widespread skeletal and multiorgan metastatic potential of human prostate cancer. This new model, reflecting the clinical situation, should be very useful for study of the biology of androgen-independent prostate cancer that is metastatic to the bone and for development of therapy for this disease.

Materials and Methods

GFP Expression Vector. pLEIN was purchased from Clontech (Palo Alto, CA). The pLEIN vector expresses enhanced GFP and the neomycin resistance gene on the same bicistronic message that contains an internal ribosome entry site (IRES) site (19).

Cell Culture, Vector Production, Transfection, and Subcloning. PT67, an NIH3T3-derived packaging cell line, expressing the 10 A1 viral envelope, was purchased from Clontech. PT67 cells were cultured in DMEM (Irvine Scientific, Santa Ana, CA) supplemented with 10% heat-inactivated fetal bovine serum (Gemini Bio-products, Calabasas, CA). For vector production, packaging cells (PT67), at 70% confluence, were incubated with a precipitated mixture of *N*-[1-(2,3-dioleoyloxy)propyl]-*N,N,N*-trimethylammoniummethyl sulfate reagent (Boehringer Mannheim) and saturating amounts of pLEIN plasmid for 18 h. Fresh medium was replenished at this time. The cells were examined by fluorescence microscopy 48 h posttransfection. For selection, the cells were cultured in the presence of 200–1000 $\mu\text{g/ml}$ G418 (potency, >45%; Life Technologies, Inc., Grand Island, NY) for 7 days.

GFP Gene Transduction of PC-3 Cells. For GFP gene transduction, 20% confluent PC-3 cells were incubated with a 1:1 precipitated mixture of retroviral supernatants of PT67 cells and Ham's F-12 K (Life Technologies, Inc.) containing 7% fetal bovine serum (Gemini Bio-products) for 72 h. Fresh medium was replenished at this time. PC-3 cells were harvested by trypsin-EDTA 72 h posttransduction and subcultured at a ratio of 1:15 into selective medium that contained 200 $\mu\text{g/ml}$ G418. The level of G418 was increased to 1000 $\mu\text{g/ml}$ stepwise. The brightest PC-3 clones expressing GFP (PC-3-GFP) were selected, combined, and then amplified and transferred by conventional culture methods.

Doubling Time of Stable GFP Clones. PC-3-GFP or nontransduced cells were seeded at 1.5×10^4 in 35-mm culture dishes. The cells were harvested and counted every 24 h using a hemocytometer (Reichert Scientific Instruments, Buffalo, NY). The doubling time was calculated from the cell growth curve over a period of 10 days.

³ The abbreviations used are: GFP, green fluorescent protein; SOI, surgical orthotopic implantation; RT-PCR, reverse transcription-PCR.

Received 10/27/98; accepted 1/4/99.

The costs of publication of this article were defrayed in part by the payment of page charges. This article must therefore be hereby marked *advertisement* in accordance with 18 U.S.C. Section 1734 solely to indicate this fact.

¹ This study was supported in part by National Cancer Institute Small Business Innovative Research Grant R44 CA53963.

² To whom requests for reprints should be addressed, at AntiCancer, Inc., 7917 Ostrow Street, San Diego, CA 92111. Phone: (619) 654-2555; Fax: (619) 268-4175; E-mail: all@anticancer.com.

s.c. Tumor Growth. Three 6-week-old BALB/c *nu/nu* male mice were injected s.c. with a single dose of 5×10^6 PC-3-GFP cells selected by high fluorescence, as described above. Cells were first harvested by trypsinization and washed three times with cold serum-free medium and then injected in a total volume of 0.2 ml within 40 min of harvesting. The nude mice were sacrificed to harvest the tumor fragments 6 weeks after tumor cell injection.

SOI. Two tumor fragments (1 mm^3) from a high GFP-fluorescent s.c. tumor from a single animal were implanted by SOI in the dorsolateral lobe of the prostate in each of five nude mice. After proper exposure of the bladder and prostate following a lower midline abdominal incision, the capsule of the prostate was opened, and the two tumor fragments were inserted into the capsule. The capsule was then closed with an 8-0 surgical suture. The incision in the abdominal wall was closed with a 6-0 surgical suture in one layer (7, 8). The animals were kept under isoflurane anesthesia during surgery. All procedures of the operation described above were performed with a $7\times$ magnification microscope (Olympus).

Analysis of Metastases. From 47 to 61 days (Table 1) after orthotopic implantation, the performance status in the mice began to decrease, at which time the animals were sacrificed and autopsied. The orthotopic primary tumor and all major organs as well as the whole skeleton were explored. The fresh samples were sliced at $\sim 1 \text{ mm}$ thickness and observed directly under fluorescence microscopy without any processing.

Microscopy. Light and fluorescence microscopy was carried out using a Nikon microscope equipped with a xenon lamp power supply. A Leica stereo fluorescence dissecting microscope model LZ12 equipped with a mercury lamp power supply was also used. Both microscopes had a GFP filter set (Chroma Technology, Brattleboro, VT). Photomicrographs were processed for brightness and contrast with Image Pro Plus Version 3.0 software (Media Cybernetics, Silver Spring, MD).

Results and Discussion

Isolation of Stable High-Level Expression GFP Transductants of PC-3 Cells. The GFP- and neomycin-containing expression vector-transduced cells were able to grow in levels of G418 up to $1000 \mu\text{g/ml}$. The selected G418-resistant PC-3 cells had a striking bright GFP fluorescence (Fig. 1a). There was no difference in the cell proliferation rates of parental cells and selected transductants determined by comparing their growth rate in monolayer culture (data not shown).

Stable High-Level Expression of GFP in PC-3 Tumors Growing s.c. in Nude Mice. Six weeks after s.c. injection of PC-3 cells, the mice were sacrificed. The tumor tissue was strongly fluorescent, thereby demonstrating stable high-level GFP expression *in vivo* during tumor growth (data not shown). Except for the lung and inguinal and iliac lymph nodes, no obvious GFP fluorescent metastases were found in systemic organs in the s.c. tumor model (data not shown).

Bone and Visceral Metastasis Visualized by GFP after Orthotopic Tumor Progression. Five of five mice developed strongly fluorescent orthotopic tumors (Fig. 1b). Three of five tumors metastasized to the skeletal system. The skeletal metastasis included the skull, rib, pelvis, femur, and tibia. Fig. 2 shows examples of tumor metastases in the skeletal system visualized by GFP. Fig. 2a shows the skull involved with metastatic prostate tumor. Fig. 2b shows the surface of the rib that is involved with tumor. In Fig. 2c, no metastatic lesions can be seen in the rib under bright-field microscopy. Fig. 2d shows the rib in the same field as Fig. 2c, under fluorescence microscopy where a strongly GFP-fluorescent metastasis can be visualized in the rib. Fig. 2, e and f, shows the prostate tumor metastasis in the pelvis, which is one of the most common metastatic sites of clinical prostate cancer. Fig. 2g shows the surface of the epiphysis of the femur. No metastatic lesions are visualized on the surface under bright-field microscopy. Fig. 2h shows the same field as Fig. 2g under fluorescence microscopy where a strongly GFP-fluorescent metastasis can be visualized on the surface of the epiphysis of the femur.

All of the tumors (5) metastasized to the lung, pleural membrane,

and kidney. Four of five tumors metastasized to liver and two of five tumors metastasized to the adrenal gland. In two mice, cancer cells or small colonies could even be seen in the brain, and in one mouse, a few cells could be seen in the spinal cord by GFP fluorescence (Fig. 3 and Table 1).

Many efforts have been made to develop an *in vivo* human prostate cancer model that closely mimics the natural history of human prostate cancer. In the last several years, orthotopic models have been established (6, 8–13). A number of experimental bone metastasis models have also been developed in the last several years (5–7, 13, 20–24). Human prostate cancer cells lines, when injected s.c. (13), orthotopically (13), i.v. including inferior vena cava occlusion (5, 21), or intraosseously (7, 23), result in skeletal metastases or intraosseous tumor growth (7). For example, as mentioned above, Thalmann *et al.* (13) injected a subline (C4-2) of LNCaP human prostate carcinoma cells into the dorsolateral lobe of the prostate gland of athymic mice. Bone metastases were detected by paraplegia in 10 and 21.5% of intact and castrated hosts, respectively, with an average latent period of 6.8 months (13). Thalmann *et al.* (13) produced the C4-2 subline by what they termed a cell-cell recombination model in which they coinjected the LNCaP cell with nontumorigenic fibroblasts from a human osteosarcoma (13, 22). A human patient prostate cancer xenograft, implanted s.c. in SCID mice, developed micrometastases in the bone marrow that were detected by the RT-PCR (24).

As mentioned above, RT-PCR was necessary (20, 24) to detect prostate cancer cells in the bone marrow; in some cases, bone scans were used for detection (7). Detection of bone and other metastases is of much lower resolution in these models than this model, in which a single GFP-expressing cell can be visualized in live fresh tissue, as seen in Fig. 3.

In this study, we established a spontaneous bone metastasis mouse model of human prostate cancer with the combination of GFP expression and SOI technique. In this model, the GFP expression of the SOI-implanted PC-3 cell line enabled metastases to be visualized throughout the skeletal system and to other important organs as well. Extensive and widespread skeletal metastases, visualized by GFP expression, were found in 60% of the animals explored. Metastases in the transplanted animals were also found in the lung, pleural membrane, liver, kidney, adrenal gland, brain, and spinal cord. Thus, the metastatic pattern of human prostate cancer PC-3-GFP accurately reproduces the clinical course of advanced metastatic androgen-independent prostate cancer. In this investigation, the extensive metastatic process in the skeleton and other organs, including the micrometastases in brain and spinal cord, was revealed by GFP fluorescence. These data demonstrate the far-reaching malignancy of this tumor, and the metastatic sites match the clinical situation. Prostate cancer mainly metastasizes to lymph nodes and bone in patients. But it also metastasizes to the other organs, such as lung, liver, pancreas, adrenal gland, large bowel, ureters, central nervous system, and so on (25, 26).

Here, we found micrometastasis in the kidney by GFP visualization. This may initiate further study of occult micro-metastasis of prostate cancer in the kidney. This may be a factor in the transfer of cancer to patients who are recipients of kidney and other transplants (27).

Such a high incidence of skeletal and other metastases could not have been previously visualized before the development of the GFP-SOI model described here.

It is possible that growth of the primary GFP-PC-3 orthotopic tumor, previously grown s.c. could have influenced the metastasis pattern, growth, or dormancy of the GFP-PC-3 cells due to angiogenic or other effects as was previously observed with the Lewis lung carcinoma (28). GFP expression could allow the effects of the primary tumor on the metastases to be even seen in the live animal, because

Table 1 *Metastatic sites of GFP-expressing human prostate cancer*

GFP-expressing PC-3 tumor tissue was transplanted by surgical orthotopic implantation in the prostate of five nude mice. The animals were sacrificed from 47 to 61 days after SOI, when the performance status began to decrease, and were explored by fluorescence microscopy for GFP-fluorescent tumor deposits.

Mouse no.	Sacrifice time (days)	Primary tumor weight (mg)	Tumor spread							
			Skeletal system	Brain	Spinal cord	Lung	Pleural membrane	Liver	Kidney	Adrenal gland
1	47	4370	+ skull, rib	+	-	+	+	+	+	+
2	47	3380	-	+	-	+	+	+	+	-
3	47	5132	-	-	+	+	+	+	+	-
4	54	5653	+ skull, pelvis, rib	-	-	+	+	-	+	+
5	61	4659	+ femurs, tibia	-	-	+	+	+	+	-

GFP expression is visualized in live tissue. Future experiments will address this point by resection of the primary tumor at various time points.

Although autofluorescence exists in various tissues, it does not interfere with the visualization of GFP-expressing tumor cells *in vivo* since tissue autofluorescence is much weaker than GFP and has emission at various wavelengths depending on the tissue. For example, in this study, the brain and spinal cord, Fig. 3, *f* and *g*, respec-

tively, show a high background of autofluorescence, but even single GFP-expressing tumor cells can still be distinguished clearly. Thus, GFP visualization of tumor metastasis has higher resolution and is much more facile than the traditional cumbersome pathological examination procedures, such as histology and immunohistochemistry or intricate molecular techniques such as RT-PCR.

The present study revealed that the bone microenvironment in the mouse provides a highly fertile soil for human prostate cancer matching

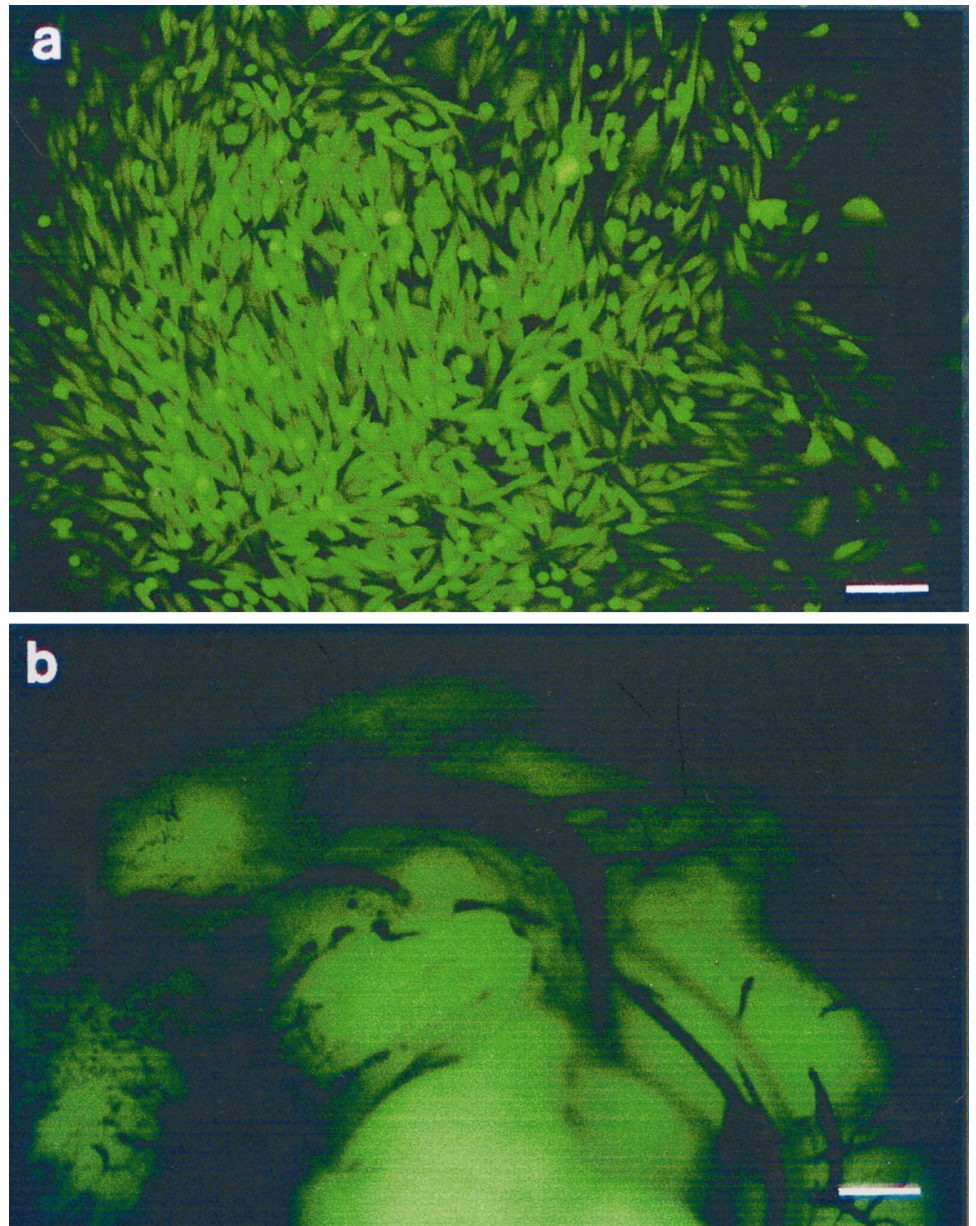


Fig. 1. Stable high-level GFP-expression of human prostate cancer PC-3 transductants, *in vitro* and *in vivo*. *a*, the human prostate cancer cell line PC-3 was transduced with the pLEIN vector that expresses enhanced GFP and the neomycin resistance genes on the same bicistronic message. Stable high-expression clones were selected in 1000 $\mu\text{g/ml}$ G418. Scale bar, 80 μm . *b*, PC-3 GFP orthotopic tumor with intense expression of GFP in the nude mouse. Scale bar, 1280 μm .

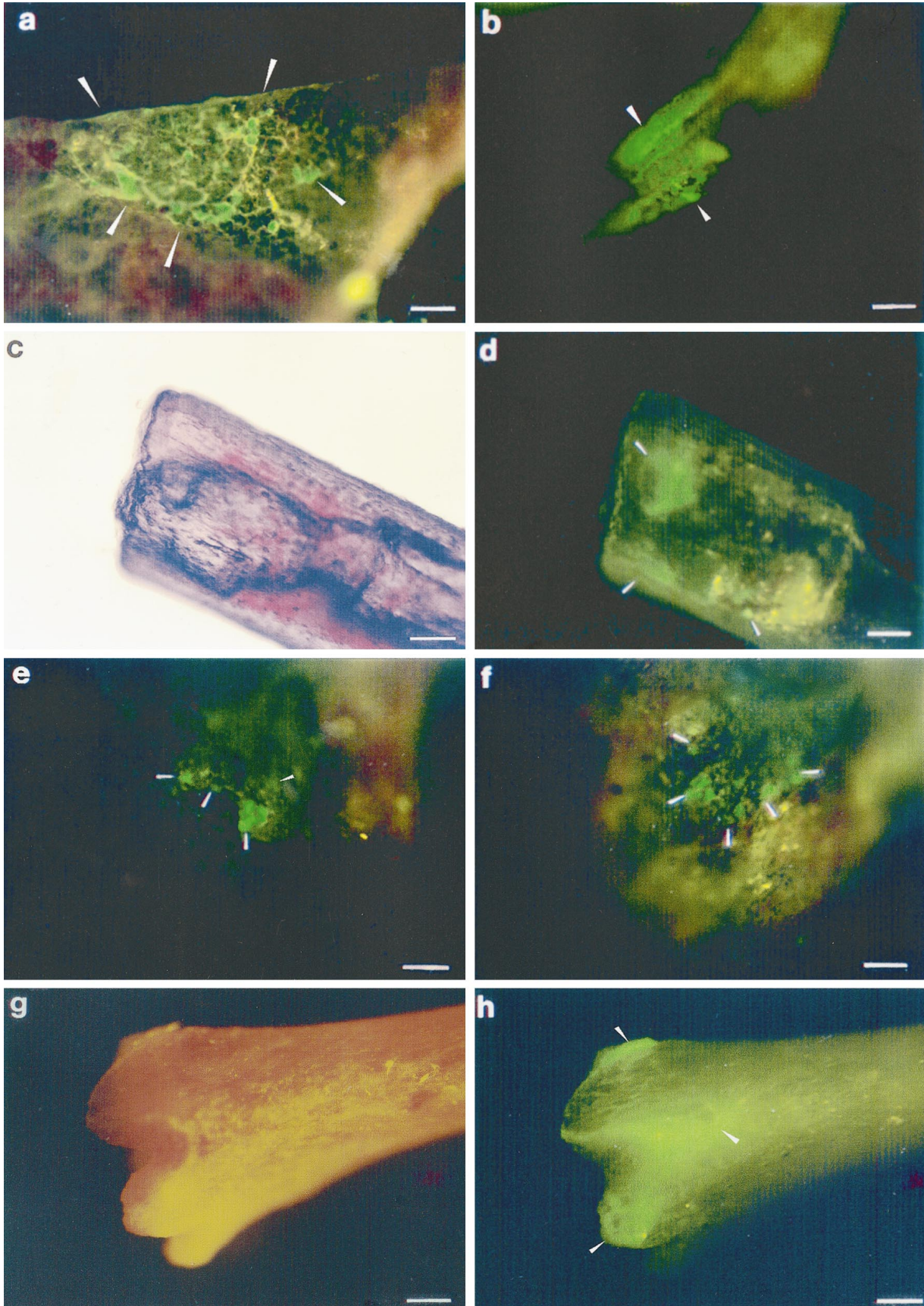


Fig. 2. Skeletal metastases of human prostate cell line PC-3 visualized by GFP expression. *a*, tumor metastasis visualized in the skull under fluorescence microscopy (arrows). Scale bar, 80 μ m. *b*, tumor metastasis visualized in the rib under fluorescence microscopy (arrows). Scale bar, 200 μ m. *c*, no metastatic lesion was visualized in the rib under bright-field microscopy. Scale bar, 80 μ m. *d*, tumor metastasis visualized in the rib under fluorescence microscopy (arrows) in the same field as *c*. Scale bar, 80 μ m. *e* and *f*, tumor metastasis visualized in the pelvis under fluorescence microscopy (arrows). Scale bar, 80 μ m. *g*, femur: no metastatic lesion was visualized in the bone marrow under bright-field microscopy. Scale bar, 320 μ m. *h*, same field as *g* under fluorescence microscopy (arrows). Strong GFP-fluorescent metastasis could be detected in the femur. Scale bar, 320 μ m.

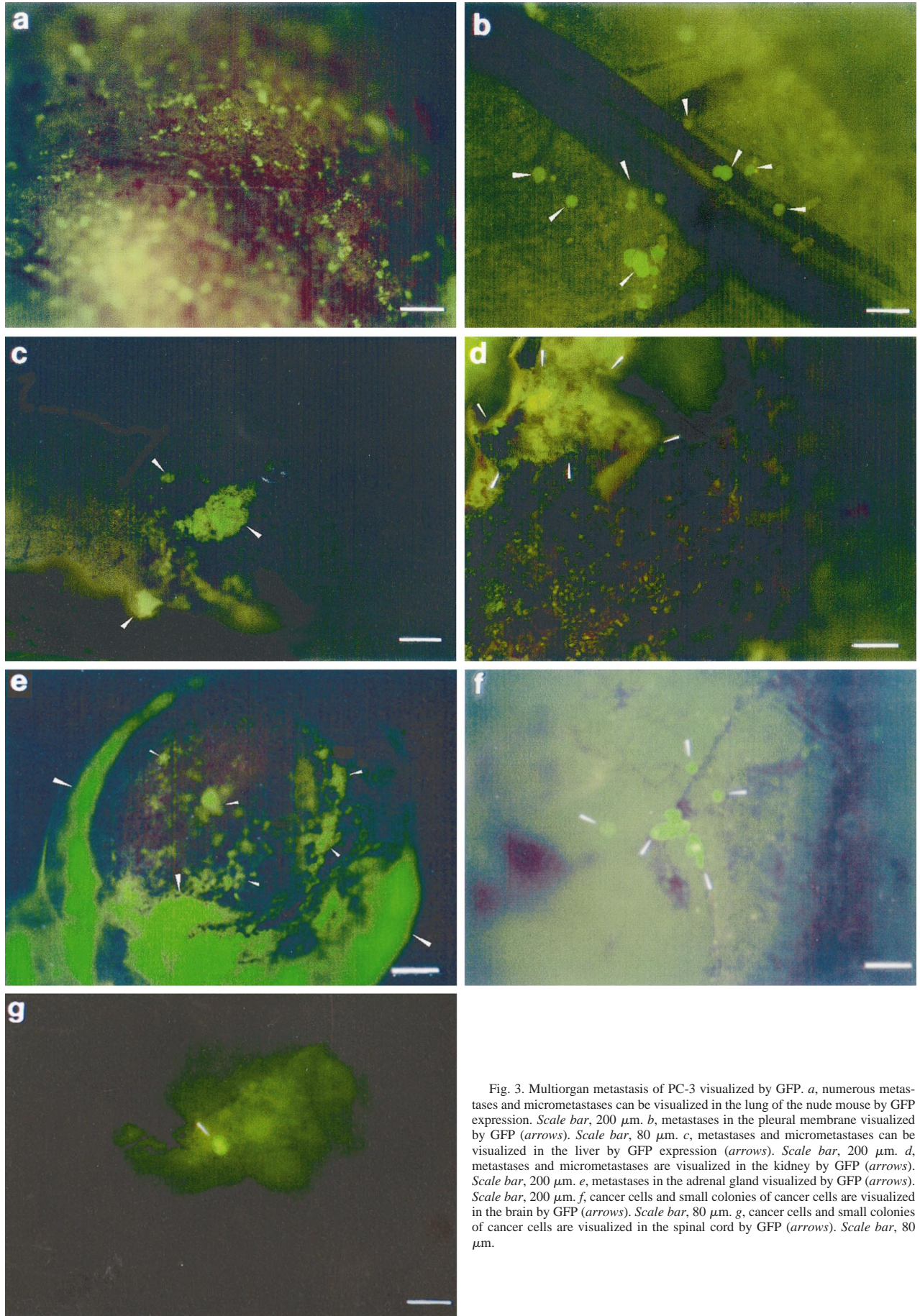


Fig. 3. Multiorgan metastasis of PC-3 visualized by GFP. *a*, numerous metastases and micrometastases can be visualized in the lung of the nude mouse by GFP expression. *Scale bar*, 200 μm . *b*, metastases in the pleural membrane visualized by GFP (arrows). *Scale bar*, 80 μm . *c*, metastases and micrometastases can be visualized in the liver by GFP expression (arrows). *Scale bar*, 200 μm . *d*, metastases and micrometastases are visualized in the kidney by GFP (arrows). *Scale bar*, 200 μm . *e*, metastases in the adrenal gland visualized by GFP (arrows). *Scale bar*, 200 μm . *f*, cancer cells and small colonies of cancer cells are visualized in the brain by GFP (arrows). *Scale bar*, 80 μm . *g*, cancer cells and small colonies of cancer cells are visualized in the spinal cord by GFP (arrows). *Scale bar*, 80 μm .

the clinical situation (25, 26). Future studies, taking advantage of GFP expression, will be performed to determine the clonogenicity of the bone metastasis. The PC-3-GFP model also revealed, for the first time, the extensive spontaneous liver metastasis potential of this tumor. This new metastatic model will be useful for studying the mechanism and developing therapy of skeletal and other metastases in prostate cancer.

References

- Boring, C. C., Squines, T. S., Tong, T., and Montgomery, S. Cancer statistics. *CA Cancer J. Clin.*, *44*: 7–26, 1994.
- Lepor, H., Ross, A., and Walsh, P. C. The influence of hormonal therapy on survival of men with advanced prostatic cancer. *J. Urol.*, *128*: 335–340, 1982.
- Kozlowski, J. M., Fidler, I. J., Campbell, D., Xu, Z., Kaighn, M. E., and Hart, L. R. Metastatic behavior of human tumor cell lines grown in the nude mouse. *Cancer Res.*, *44*: 3522–3529, 1984.
- Kaighn, M. E., Narayan, K. S., Ohnuki, Y., Lechner, J. F., and Jones, L. W. Establishment and characterization of a human prostate carcinoma cell line (PC-3). *Invest. Urol.*, *17*: 16–23, 1979.
- Shevrin, D. H., Kukreja, S. C., Ghosh, L., and Lad, T. E. Development of skeletal metastasis by human prostate cancer in athymic nude mice. *Clin. Exp. Metastasis*, *6*: 401–409, 1988.
- Pettaway, C. A., Pathak, S., Greene, G., Ramirez, E., Wilson, M. R., Killion, J. J., and Fidler, I. J. Selection of highly metastatic variants of different human prostatic carcinomas using orthotopic implantation in nude mice. *Clin. Cancer Res.*, *2*: 1627–1636, 1996.
- Wu, T. T., Sike, R. A., Cui, Q., Thalmann, G. N., Kao, C., Murphy, C. F., Yang, H., Zhau, H. E., Balian, G., and Chung, L. W. Establishing human prostate cancer cell xenografts in bone: induction of osteoblastic reaction by prostate-specific antigen-producing tumors in athymic and SCID/bg mice using LNCaP and lineage-derived metastatic sublines. *Int. J. Cancer*, *77*: 887–894, 1998.
- Stephenson, R. A., Dinney, C. P. N., Gohji, K., Ordonez, N. G., Killion, J. J., and Fidler, I. J. Metastasis model for human prostate cancer using orthotopic implantation in nude mice. *J. Natl. Cancer Inst. (Bethesda)*, *84*: 951–957, 1992.
- Fu, X., Herrera, H., and Hoffman, R. M. Orthotopic growth and metastasis of human prostate carcinoma in nude mice after transplantation of histologically intact tissue. *Int. J. Cancer*, *52*: 987–990, 1992.
- Saito, N., Gleave, M. E., Bruchovshy, N., Rennie, P. S., Beraldi, E., and Sullivan, L. D. A metastatic and androgen-sensitive human prostate cancer model using intraprostatic inoculation of LNCaP cells in SCID mice. *Cancer Res.*, *57*: 1584–1589, 1997.
- Rembrink, K., Romijn, J. C., van der Kwast, T. H., Rubben, H., and Schroder, F. H. Orthotopic implantation of human prostate cancer cell lines: a clinically-relevant animal model for metastatic prostate cancer. *Prostate*, *31*: 168–174, 1997.
- An, Z., Wang, X., Geller, J., Moossa, A. R., and Hoffman, R. M. Surgical orthotopic implantation allows high lung and lymph node metastatic expression of human prostate carcinoma cell line PC-3 in nude mice. *Prostate*, *34*: 169–174, 1998.
- Thalmann, G. N., Anezinis, P. E., Chang, S. M., Zhou, H. E., Kim, E. E., Hopwood, V. L., Pathak, S., Eschenbach, A. C. V., and Chung, W. K. Androgen-independent cancer progression and bone metastasis in the LNCaP model of human cancer. *Cancer Res.*, *54*: 2577–2581, 1994.
- Chishima, T., Miyagi, Y., Wang, X., Yamaoka, H., Shimada, H., Moossa, A. R., and Hoffman, R. M. Cancer invasion and micrometastasis visualized in live tissue by green fluorescent protein expression. *Cancer Res.*, *57*: 2042–2047, 1997.
- Chishima, T., Miyagi, Y., Wang, X., Tan, Y., Shimada, H., Moossa, A. R., and Hoffman, R. M. Visualization of the metastatic process by green fluorescent protein expression. *Anticancer Res.*, *17*: 2377–2384, 1997.
- Chishima, T., Miyagi, Y., Wang, X., Baranov, E., Tan, Y., Shimada, H., Moossa, A. R., and Hoffman, R. M. Metastatic patterns of lung cancer visualized live and in process by green fluorescence protein expression. *Clin. Exp. Metastasis*, *15*: 547–552, 1997.
- Chishima, T., Miyagi, Y., Li, L., Tan, Y., Baranov, E., Yang, M., Shimada, H., Moossa, A. R., and Hoffman, R. M. Use of histoculture and green fluorescent protein to visualize tumor cell host interaction. *In Vitro Cell Dev. Biol.*, *33*: 745–747, 1997.
- Chishima, T., Yang, M., Miyagi, Y., Li, L., Tan, Y., Baranov, E., Shimada, H., Moossa, A. R., and Hoffman, R. M. Governing step of metastasis visualized *in vitro*. *Proc. Natl. Acad. Sci. USA*, *94*: 11573–11576, 1997.
- Yang, M., Hasegawa, S., Jiang, P., Wang, X., Tan, Y., Chishima, T., Shimada, H., Moossa, A. R., and Hoffman, R. M. Widespread skeletal metastatic potential of human lung cancer revealed by green fluorescent protein expression. *Cancer Res.*, *58*: 4217–4221, 1998.
- Dolman, C. S., Mueller, B. M., Lode, H. N., Xiang, R., Gillies, S. D., and Reisfeld, R. A. Suppression of human prostate carcinoma metastases in severe combined immunodeficient mice by interleukin-2 immunocytokine therapy. *Clin. Cancer Res.*, *4*: 2551–2557, 1998.
- Wang, M., and Stearns, M. E. Isolation and characterization of PC-3 human prostatic tumor sublines which preferentially metastasize to select organs in SCID mice. *Differentiation*, *48*: 115–125, 1991.
- Wu, H. C., Hsieh, J. T., Gleave, M. E., Brown, N. M., Pathak, S., and Chung, L. W. Derivation of androgen-independent human LNCaP prostatic cancer cell sublines: role of bone stromal cells. *Int. J. Cancer*, *57*: 406–412, 1994.
- Soos, G., Zukowski, K., Jones, R. F., Haas, G. P., and Wang, C. Y. Heterotopic growth of human prostate carcinoma in the femurs of nude mice: an osseous metastatic model. *Int. J. Cancer*, *66*: 280–281, 1996.
- Klein, K., Reiter, R., Redulla, J., Moradi, H., Zhu, X., Brothman, A., Lamb, D., Marcelli, M., Bellegrun, A., Witte, O., and Sawyers, C. Progression of metastatic human prostate cancer to androgen independence in immunodeficient SCID mice. *Nat. Med.*, *3*: 402–408, 1997.
- De la Monte, S. M., Moore, G. W., and Hutchins, G. M. Metastatic Behavior of prostate cancer. Cluster analysis of patterns with respect to estrogen treatment. *Cancer (Phila.)*, *58*: 985–993, 1986.
- Mundy, G. R. Mechanisms of bone metastasis. *Cancer (Phila.)*, *80*: 1546–1556, 1997.
- Lawrence, S. K., Van Buren, D. H., MacDonell, R. C., Jr., and Delbeke, D. Carcinoma in a transplanted kidney detected with MAG3 scintigraphy. *J. Nucl. Med.*, *34*: 2185–2187, 1993.
- O'Reilly, M. S., Holmgren, L., Shing, Y., Chen, C., Rosenthal, R. A., Moses, M., Lane, W. S., Cao, Y., Sage, E. H., and Folkman, J. Angiostatin: a novel angiogenesis inhibitor that mediates the suppression of metastases by a Lewis lung carcinoma. *Cell*, *79*: 315–328, 1994.